




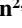


## Impacts of Initial Zonal Current Errors on the Predictions of Two Types of El Niño Events

Lingjiang Tao<sup>1,2</sup> , Mu Mu<sup>3</sup> , Lei Wang<sup>3</sup> , Xianghui Fang<sup>3</sup> , Wansuo Duan<sup>2,4</sup> , and Rong-Hua Zhang<sup>1,4</sup> 

<sup>1</sup>School of Marine Sciences, Nanjing University of Information Science and Technology, Nanjing, China, <sup>2</sup>LASG, Institute of Atmospheric Physics, Chinese Academy of Sciences, Beijing, China, <sup>3</sup>Department of Atmospheric and Oceanic Sciences & Institute of Atmospheric Sciences, Fudan University, Shanghai, China, <sup>4</sup>University of Chinese Academy of Sciences, Beijing, China

### Key Points:

- The initial zonal current errors in the central and western tropical Pacific have the severest impact on the El Niño prediction
- The impact of the initial zonal current errors on the central Pacific (CP) El Niño prediction is greater than on the eastern Pacific (EP) El Niño prediction
- The initial zonal current errors can induce the fastest error growth in spring (summer) during the EP (CP) El Niño prediction

### Supporting Information:

Supporting Information may be found in the online version of this article.

### Correspondence to:

L. Tao,  
taolj1992@foxmail.com

### Citation:

Tao, L., Mu, M., Wang, L., Fang, X., Duan, W., & Zhang, R.-H. (2023). Impacts of initial zonal current errors on the predictions of two types of El Niño events. *Journal of Geophysical Research: Oceans*, 128, e2023JC019833. <https://doi.org/10.1029/2023JC019833>

Received 14 MAR 2023

Accepted 14 JUN 2023

### Author Contributions:

**Conceptualization:** Lingjiang Tao, Mu Mu, Wansuo Duan, Rong-Hua Zhang  
**Data curation:** Lingjiang Tao, Lei Wang  
**Formal analysis:** Lingjiang Tao, Xianghui Fang, Rong-Hua Zhang  
**Funding acquisition:** Lingjiang Tao, Mu Mu, Lei Wang, Rong-Hua Zhang  
**Investigation:** Lingjiang Tao  
**Methodology:** Lingjiang Tao, Mu Mu, Wansuo Duan  
**Resources:** Lingjiang Tao  
**Software:** Lingjiang Tao  
**Supervision:** Mu Mu, Lei Wang  
**Validation:** Lingjiang Tao  
**Visualization:** Lingjiang Tao  
**Writing – original draft:** Lingjiang Tao  
**Writing – review & editing:** Lingjiang Tao, Mu Mu, Lei Wang, Xianghui Fang, Wansuo Duan, Rong-Hua Zhang

**Abstract** Perturbations in the thermocline and surface zonal current (ZC) play crucial roles in the evolutions of the eastern Pacific (EP) and central Pacific (CP) El Niño events, respectively. Whereas numerous studies have examined the influence of initial uncertainties in ocean temperature on the predictability of El Niño, only a few studies investigated the impact of the initial ZC. Using an air-sea coupling model, the conditional nonlinear optimal perturbation (CNOP) approach was employed to investigate the maximum impact of initial ZC errors on the El Niño prediction. The optimal initial ZC errors (denoted as CNOP-U<sub>s</sub>) that have the severest impact on the El Niño prediction are found to mainly concentrate in the western and central tropical Pacific. The CNOP-U<sub>s</sub> cause larger errors in the CP El Niño prediction than in the EP El Niño prediction. Additionally, CNOP-U<sub>s</sub> cause rapid sea surface temperature error growth in spring in the EP El Niño prediction but in summer in the CP El Niño prediction. Dynamically, the former is related to the large uncertainties in the meridional current in spring caused by CNOP-U<sub>s</sub>, while the latter is related to the strong ZC errors in summer. According to the distributions of CNOP-U<sub>s</sub>, reducing the initial ZC errors in the western and central tropical Pacific may be vital in weakening the predictability barrier phenomena and improving the predictions of El Niño diversity.

**Plain Language Summary** Investigating the relationship between the prediction error and initial error is conducive to studying the predictability of El Niño and its sources of prediction errors. A lot of effort has been made on investigating the predictability of El Niño to the initial errors in ocean temperature. However, as another factor influencing the growth of El Niño, the impact of the initial zonal current (ZC) errors on the El Niño prediction are less concerned. Therefore, the present study investigates the largest-growing error mode in the ZC for CP and EP El Niño predictions by using the conditional nonlinear optimal perturbation (CNOP) approach. We found that the CP El Niño prediction is more sensitive to the initial ZC than the EP El Niño prediction. Both the spring predictability barrier (PB) of the EP El Niño prediction and the summer PB of the CP El Niño prediction are attributed to the initial errors in the ZC in the central and eastern tropical Pacific. The spring (summer) PB for EP (CP) El Niño is caused by the CNOP-U<sub>s</sub>-induced uncertainties in the meridional (zonal) advection in the eastern (central) tropical Pacific. The former results can further improve the understanding of the predictability of El Niño diversity.

## 1. Introduction

The El Niño Southern Oscillation (ENSO), which occurs in the tropical Pacific, is a commonplace climate phenomenon with a period of 2 to 7 years (Philander, 1983). Because of its tremendous effect on the global weather and climate, every El Niño outbreak has always attracted large attention to the public, especially climatologists (e.g., Alexander et al., 2002; Gao et al., 2022; McPhaden, 2015; Zhang & Gao, 2016). Since the pioneering study of Bjerknes (1969) on the ENSO dynamics, great progress has been achieved in understanding the El Niño event using various models and increased observations (see a review by Fang and Xie (2020)). At present, ENSO prediction is one of the most successful cases of short-term climate predictions whose effectiveness can reach more than 6 to 9 months in advance (Tang et al., 2018; Zhou & Zhang, 2022).

Nevertheless, real-time predictions of ENSO still face many problems that need to be solved (Zhang et al., 2022). For example, the spring predictability barrier (PB), which is a well-known phenomenon indicating that the

prediction skill usually rapidly drops during boreal spring, makes ENSO prediction difficult (Jin et al., 2008; Webster & Yang, 1992). From the perspective of prediction error growth, such seasonal-dependent predictability is reflected in the rapid error growth in spring, which leads to a large error growth at the end of the prediction (Duan & Mu, 2018). Evidently, studying and reducing the PB phenomenon are important to understand the ENSO predictability and improve the ENSO prediction skill. Various studies, therefore, have been conducted to explore the spring PB phenomenon of ENSO. Some studies suggest that spring PB is an intrinsic property of ENSO, for example, it is attributed to weak air–sea coupling, small growth rate, and lowest signal-to-noise ratio during this season (Levine & McPhaden, 2015; Liu et al., 2019; Torrence & Webster, 1998; Zheng et al., 2016).

Many studies have determined that the initial errors of ENSO models play an important role in the spring PB phenomenon. Because the thermocline (or subsurface temperature) fluctuation and sea-surface temperature (SST) perturbation are key oceanic factors that result in El Niño generation (Jin, 1997), previous studies mainly focused on the roles of initial uncertainties in the thermocline depth and SST in El Niño predictability (Lee et al., 2018; Moore & Kleeman, 1996; Tao et al., 2017; Yang et al., 2020; Yu et al., 2009). For instance, based on the conditional nonlinear optimal perturbation (CNOP) approach (Mu et al., 2003) and the Zebiak–Cane model (Zebiak & Cane, 1987), Mu et al. (2007) discovered that the largest growing type of initial condition error characterizes a basin-scale-deepened thermocline and a dipole pattern of equatorial SST errors (positive errors in the east and negative errors in the central and western tropical Pacific). Such types of initial errors can induce the fastest error growth in spring, thereby seriously destroying the ENSO prediction and leading to large uncertainties at the end of the prediction. By employing a general circulation model, Duan and Hu (2016) investigated the spring PB-related initial temperature errors in the upper ocean and emphasized that the initial-temperature errors in the upper layers of the eastern equatorial Pacific and lower layers of the central–western equatorial Pacific are the culprits in the error growth in spring. In a sense, El Niño prediction is sensitive to the initial conditions in these regions; thus, a corresponding target observation can help reduce the spring PB phenomenon and improve ENSO prediction (Duan et al., 2018; Hou et al., 2023; Tao et al., 2018).

Note that previous studies on the ENSO predictability only focused on traditional El Niño events (i.e., SST peaks in the eastern tropical Pacific). Since the start of the 21st century, a new type of El Niño whose warming is centered in the central tropical Pacific has more frequently occurred (Gao et al., 2022; Kug et al., 2009; Yeh et al., 2009). According to the location of the warm center, these two types of El Niño are referred to as EP and CP El Niño. The CP El Niño shows distinct dynamics and predictability compared with the EP El Niño (Timmermann et al., 2018). For example, the CP El Niño is more difficult to predict than the EP El Niño using the operational models (Ren, Scaife, et al., 2018; Zheng & Yu, 2017). This low prediction skill of the CP El Niño is partly due to the changes in the sources of ENSO predictability and its relatively small amplitude (Ren, Zuo, & Deng, 2018; Tao & Duan, 2022). For example, some studies demonstrated that the CP El Niño originates from the SST–wind perturbation in the north subtropical Pacific, whereas the EP El Niño is triggered by the SST anomalies in the equatorial Atlantic (Ham et al., 2013; Yu et al., 2010). Additionally, the PB phenomenon also occurs in the CP El Niño prediction but with different timing and intensity. Compared with the spring PB of the EP El Niño, the PB of the CP El Niño is weaker and locked in summer (Hou et al., 2019; Qi et al., 2021; Ren et al., 2016; Ren, Zuo, & Deng, 2018; Tian & Duan, 2016). To investigate the distinct PB phenomena of the EP and CP El Niño, Hou et al. (2019) investigated the roles of the initial errors in the two types of El Niño predictions using a large sample of model outputs and the CNOP approach. They found that the initial SST errors in the Victoria-mode region in the North Pacific are the main sources of summer PB of the CP El Niño, whereas the initial temperature errors in the subsurface layer of the western tropical Pacific are the main sources of spring PB of the EP El Niño.

From the abovementioned information, the changes in the ENSO predictability are related to the different sensitivities to the initial ocean temperature in the two types of El Niño. In fact, the evolution of El Niño is not only related to thermodynamics but also controlled by ocean currents, especially the surface zonal current (ZC) anomaly (An et al., 1999; Delcroix et al., 1992; Hsin & Qiu, 2012; Wyrtki, 1975). For example, strong El Niño events are usually preceded by easterly ZC anomalies (Kim & Cai, 2014). The persistent eastward ZC pushes the warm pool to the central-eastern tropical Pacific and finally warms up the region. Moreover, the anomalous heat transport induced by the ZC anomaly (known as the zonal advection feedback term) plays an important role in the occurrence of El Niño diversity (Chen et al., 2022; Fang & Mu, 2018; Kug et al., 2009), especially in the CP El Niño. Therefore, the false representations of the zonal advection feedback possibly cause the current models to demonstrate low performance in simulating the two types of El Niño (Feng et al., 2020). Information on the ZC also clearly provides predictability of El Niño to a certain extent (Wang et al., 2017). Then, one can assume

that the initial ZC uncertainties may play a certain role in the uncertainties of the ENSO prediction. In particular, the initial ZC information can influence the zonal advection feedback, thus greatly contaminating the CP El Niño prediction. However, this hypothesis has not been proven yet, and how the ZC affects the predictability of the two types of El Niño remains unclear.

To this end, the present study focuses on the initial uncertainties in the ZC over the mixed layer and explores their potential effects on the prediction of various El Niño events. In this work, the CNOP approach is applied to an operational ENSO model to investigate the most-growing pattern of initial errors in the ZC (denoted as CNOP-U<sub>s</sub>) that can influence the El Niño prediction most. Then, the roles of CNOP-U<sub>s</sub> in the EP and CP El Niño predictions are demonstrated. Overall, the main purpose of the study is to address the following issues: (a) to what extent the ZC uncertainties influence the predictions of two types of El Niño and (b) whether and how the initial errors in the ZC cause seasonal-dependent error growth? Following the Introduction, a brief description of the ENSO model and CNOP approach is presented in Section 2. Section 3 describes the CNOP-U<sub>s</sub> and explains their distinct effects on the two types of El Niño predictions. Then, the dynamics of the seasonal error growth are analyzed in Section 4. Finally, a summary is provided in Section 5, together with a discussion on ENSO predictability.

## 2. Model and Method

### 2.1. ENSO Model

In this study, an intermediate coupled model (ICM) from the Institute of Oceanology, Chinese Academy of Sciences, China, is adopted to study the link between ENSO predictability and the ZC uncertainty. The ICM, developed by Zhang et al. (2003) is an air-sea coupled model made up by a wind stress model, an intermediate dynamical ocean model (IOM) and an SST anomaly model.

In the IOM, the governing equations of the ocean currents are divided into two parts: the linear (IOM-L) and nonlinear (IOM-NL) parts. The IOM-L is derived from the McCreary model (McCreary, 1981) but considers the horizontal variations of stratification. The IOM-L equations are expressed as follows:

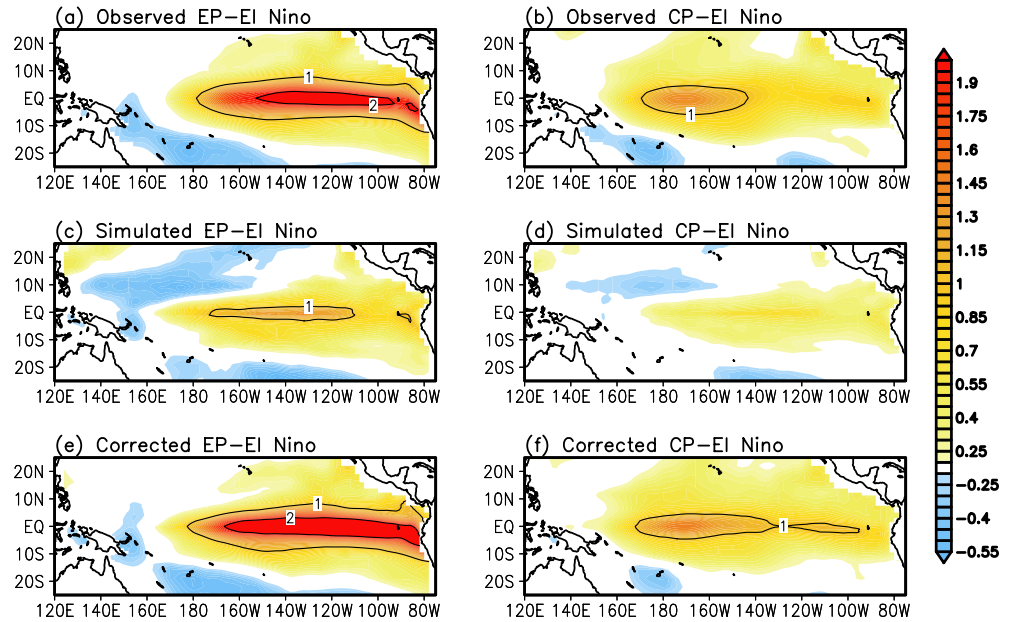
$$\begin{aligned} u_t - f v &= -p_x + v_h \nabla_h^2 u + (v_v u_z)_z \\ v_t + f u &= -p_y + v_h \nabla_h^2 v + (v_v v_z)_z \\ p_z + \rho g &= 0 \\ \nabla \cdot \bar{u} &= 0 \\ \rho_t - \frac{w}{g} N^2 &= k_h \nabla_h^2 \rho + (k_v \rho)_z \end{aligned} \quad (1)$$

where  $\bar{u} = (u, v, w)$  is the ocean current,  $f$  is the Coriolis frequency, and  $g$  is the gravitational acceleration.  $k_h$  and  $k_v$  are the horizontal and vertical eddy diffusivities of heat, respectively.  $v_h$  and  $v_v$  are the horizontal and vertical eddy diffusivities of momentum, respectively.  $p$  ( $= \frac{p}{\rho_0}$ ) is the kinematic pressure, and  $N^2$  is the background Brunt–Vaisala frequency (i.e., buoyancy frequency), which varies with space in the IOM-L. The IOM-NL represents the greatly simplified residual nonlinear momentum due to the linearization. It can be expressed as

$$\begin{aligned} u_t^{nl} + \bar{u} \cdot \nabla u &= v_h \nabla_h^2 u^{nl} + (v_v u_z^{nl})_z \\ \nabla \cdot u^{nl} &= 0 \end{aligned} \quad (2)$$

where  $u = u^{nl} + u^l$  is the total zonal velocity with nonlinear contribution  $u^{nl}$  and linear component  $u^l$  of the ZC. By combining the IOM-L and IOM-NL, the IOM can well capture the nonlinearity of the ocean current and its effect on the equatorial undercurrent and south equatorial current. A more detailed description of IOM can be found in the work of Keenlyside and Kleeman (2002).

In addition, one prominent aspect of the ICM is that the SST anomaly model is equipped with an empirically determined subsurface temperature ( $T_e$ ) model, where the  $T_e$  model illustrates the effect of the anomalous temperature of the subsurface water entrained in the mixed layer. The  $T_e$  model is established based on a global relationship between the anomalous sea level (SL) and  $T_e$  using a singular-value-decomposition approach. Because of the



**Figure 1.** Horizontal distributions of the composite sea surface temperature (SST) anomalies during the eastern Pacific (EP) and central Pacific (CP) El Niño years from October to December. The panels from top to bottom are derived from observation and 12-month simulation using intermediate coupled model (ICM) and nonlinear forcing singular vector (NFSV)-ICM. The composites are made from seven CP El Niño events and six EP El Niño events that occurred during 1980–2020 (see Table 1). The contour interval is 1°C.

close link with SL, the  $T_e$  anomaly can be appropriately estimated to well represent the thermocline effect on the ENSO evolution. Equipped with the  $T_e$  model, the variations in the SST anomaly are controlled by the following equations:

$$\begin{aligned} \frac{\partial T'}{\partial t} &= ZA + MA + VC + DF + HF \\ ZA &= -u' \frac{\partial \bar{T}}{\partial x} - \bar{u} \frac{\partial T'}{\partial x} - u' \frac{\partial T'}{\partial x} \\ MA &= -v' \frac{\partial \bar{T}}{\partial y} - \bar{v} \frac{\partial T'}{\partial y} - v' \frac{\partial T'}{\partial y} \\ VC &= -[(\bar{w} + w')M(-\bar{w} - w') - \bar{w}M(-\bar{w})] \frac{\bar{T}_e - \bar{T}}{H} - (\bar{w} + w')M(-\bar{w} - w') \frac{T'_e - T'}{H} \end{aligned} \quad (3)$$

where ZA, MA, and VC are the zonal advection, meridional advection, and vertical convection terms of the heat transport, respectively. DF and HF are the diffusion and surface heat-flux terms, respectively.  $T'_e$  and  $T'$  denote interannual anomalous  $T_e$  and SST, respectively. The detailed meanings and settings of the parameters and variables are found in the work of Keenlyside (2001).

Previous studies showed that ICM demonstrated good performance in depicting and predicting the ENSO evolutions (Zhang & Gao, 2016). Nevertheless, in practice, errors undeniably appear in simulating the El Niño events, especially the CP El Niño events, because of the large simplification of the tropical climate system (Tao et al., 2022). For example, the simulated El Niño events are usually weaker than the observed ones (Figures 1c and 1d). Moreover, the modeled CP El Niño events impractically extend eastward. To nullify the errors induced

by the simplification, an optimal forcing is added to the tendency of the SST model (Equation 3) to make the simulation approach closest to the observation results (Duan et al., 2014). The corrected SST anomaly model can then be expressed as

$$\frac{\partial T'}{\partial t} = ZA + MA + VC + DF + HF + f \quad (4)$$

where  $f$  is optimized by assimilating the observation results using the nonlinear forcing singular vector (NFSV). Figure 1 shows the performance of ICM

**Table 1**  
Years of Two Types of El Niño Identified Using the Method Proposed by Kug et al. (2009)

| Types of El Niño | Year when El Niño peaks                  |
|------------------|--|
| EP El Niño       | 1982, 1986, 1991, 1997, 2002, 2015       |
| CP El Niño       | 1987, 1994, 2004, 2006, 2009, 2014, 2018 |

that is equipped with NFSV forcing (denoted as NFSV-ICM hereafter) in simulating the EP and CP El Niño. We can see that the modeled El Niño events significantly improve and approach the observed events with equal amplitudes and similar spatial structures. The SST data used to assess the effectiveness of the NFSV assimilation come from the National Oceanic and Atmospheric Administration (NOAA) Extended Reconstructed SST V5 (Huang et al., 2017).

Owing to the advantage of the simulation in El Niño diversity and ocean currents, ICM equipped with NFSV is used as the model platform to explore the EP and CP El Niño predictability involving initial uncertainties in the ZC.

## 2.2. CNOP and Experimental Design

The CNOP approach, which was first proposed by Mu et al. (2003), aims to search for the optimal initial errors in a certain physical constraint that can cause the largest error growth in a nonlinear system. Differed to other methods, the CNOP approach can mathematically identify the most unstable initial error mode in continuous space. Hence, one can investigate the predictability limit due to the initial errors by using the CNOP approach. It has been widely used for exploring the predictability of climate and weather events owing to its advantage in exploring the sensitivity of a nonlinear system to initial conditions (e.g., Mu et al., 2007; Tao et al., 2017; Wei et al., 2019).

In the present study, the CNOP approach is applied to the corrected ICM (i.e., NFSV-ICM) to investigate the most unstable mode of initial uncertainties in the ZC. Let the solution of Equation 4 be denoted as  $T = M_t(\mathbf{f}_r, \mathbf{X}_0)$  with initial condition  $\mathbf{X}_0$  and NFSV-optimized forcing  $\mathbf{f}_r$ . If the integral starts in January of each El Niño year, and the integral time is 12 months,  $T = M_t(\mathbf{f}_r, \mathbf{X}_0)$  is the simulated SST anomaly of one observed El Niño event. The obtained  $T$  is termed as reference state. Then, a perturbation ( $\mathbf{u}$ ) that is superimposed on the initial ZC over the mixed layer leads to a new solution, which is denoted as  $T' = M_t(\mathbf{f}_r, \mathbf{X}_0 + \mathbf{u})$ . The departure of the SST anomaly induced by  $\mathbf{u}$  from the reference state is defined as the difference between  $T'$  and  $T$ . To search for optimal  $\mathbf{u}$  (denoted as  $\mathbf{u}^*$ ) that can most influence the prediction, we define the following constraint problem:

$$J(\mathbf{u}^*) = \max_{\iint u^2 dV \leq 10 \text{ m}^2/\text{s}^2} \|\mathbf{M}_t(\mathbf{f}_r, \mathbf{X}_0 + \mathbf{u}) - \mathbf{M}_t(\mathbf{f}_r, \mathbf{X}_0)\| \quad (5)$$

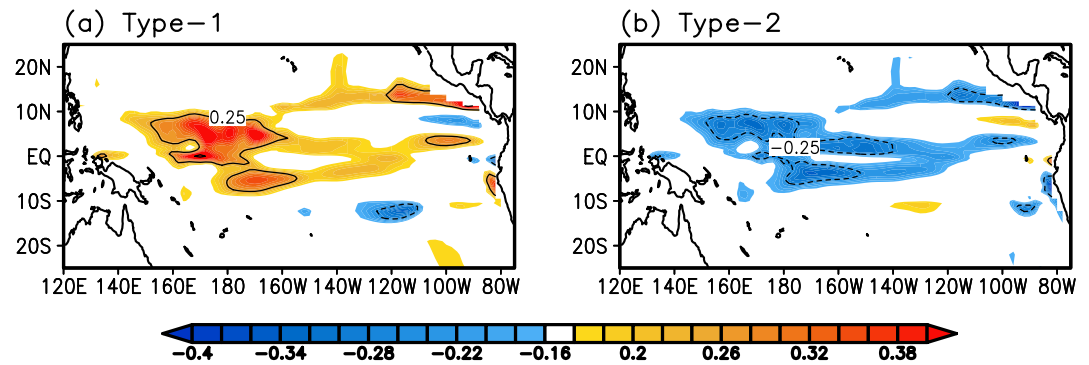
where  $J$  is the objective function that measures the error growth,  $\mathbf{u}$  is constrained by  $\iint u^2 dV \leq 10 \text{ m}^2/\text{s}^2$ , and  $\|\cdot\|$  is the L2 norm over the tropical Pacific. Here, the constraint size of  $\mathbf{u}$  is not randomly chosen but is based on the actual observation errors of the current. Undeniably, a larger (smaller) constraint leads to a larger (lesser) error growth. However, the horizontal distribution of  $\mathbf{u}^*$  hardly changes. Therefore, we only present the result with a constraint size of  $10 \text{ m}^2/\text{s}^2$ . By solving Equation 5, we can thus search for the optimal initial error in the ZC that can most influence the predictions (referred to as CNOP-U hereafter). From the above discussions, the CNOP analysis is designed to explore the most unstable error mode of the ZC at the start of the El Niño year that can induce the largest error growth in the prediction of El Niño at its mature phase.

The calculation of Equation 5 is complicated, although it has been fortunately solved using the adjoint model of ICM and an optimization algorithm (Gao et al., 2016, 2018). In consideration of the focus of this study and the length of this manuscript, such a solution is not described, but interested readers can refer to the work of Tao et al. (2017).

## 3. CNOP-U's and Their Effects on EP and CP El Niño Predictions

Thirteen El Niño events (including six EP and seven CP El Niño events, see Table 1), which occurred during the period from 1980 to 2020, are chosen to investigate their predictabilities relative to the initial errors in the ZC. Based on the CNOP approach mentioned in Section 2.1, two solutions can be obtained for each El Niño prediction: one is the global solution that represents the global largest growing error in the whole space; the other is the local solution that represents another extremum but second only to the global solution. Corresponding to 13 El Niño events, we can obtain  $13 \times 2$  CNOP-U's including global and local solutions. It is of interest that these CNOP-U's show remarkably similar patterns, but of which the global and local ones are out of phase. That is, there exist two common initial ZC errors that tend to influence the El Niño prediction most. To obtain such two kinds of the CNOP-U's, composites are made among 13 global CNOP-U's and 13 local CNOP-U's, respectively.

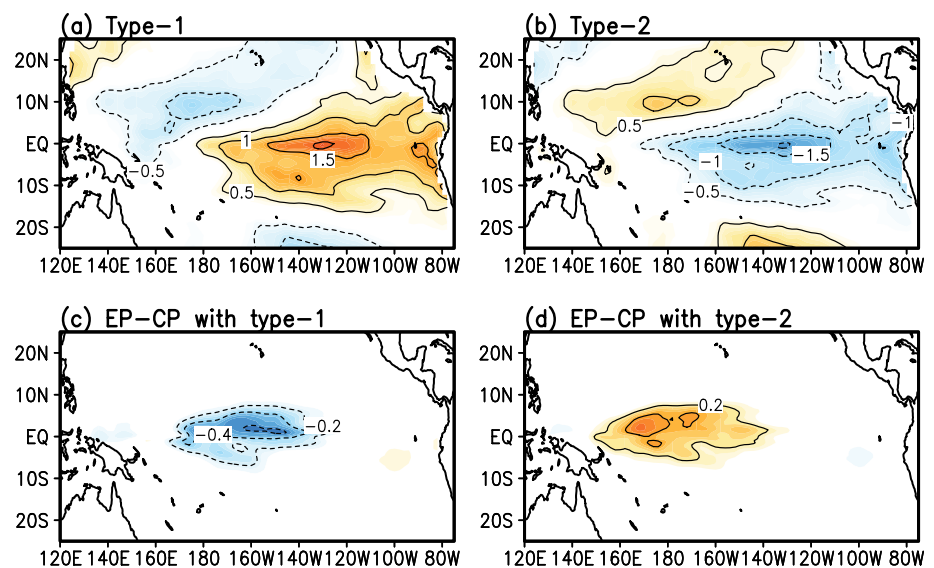




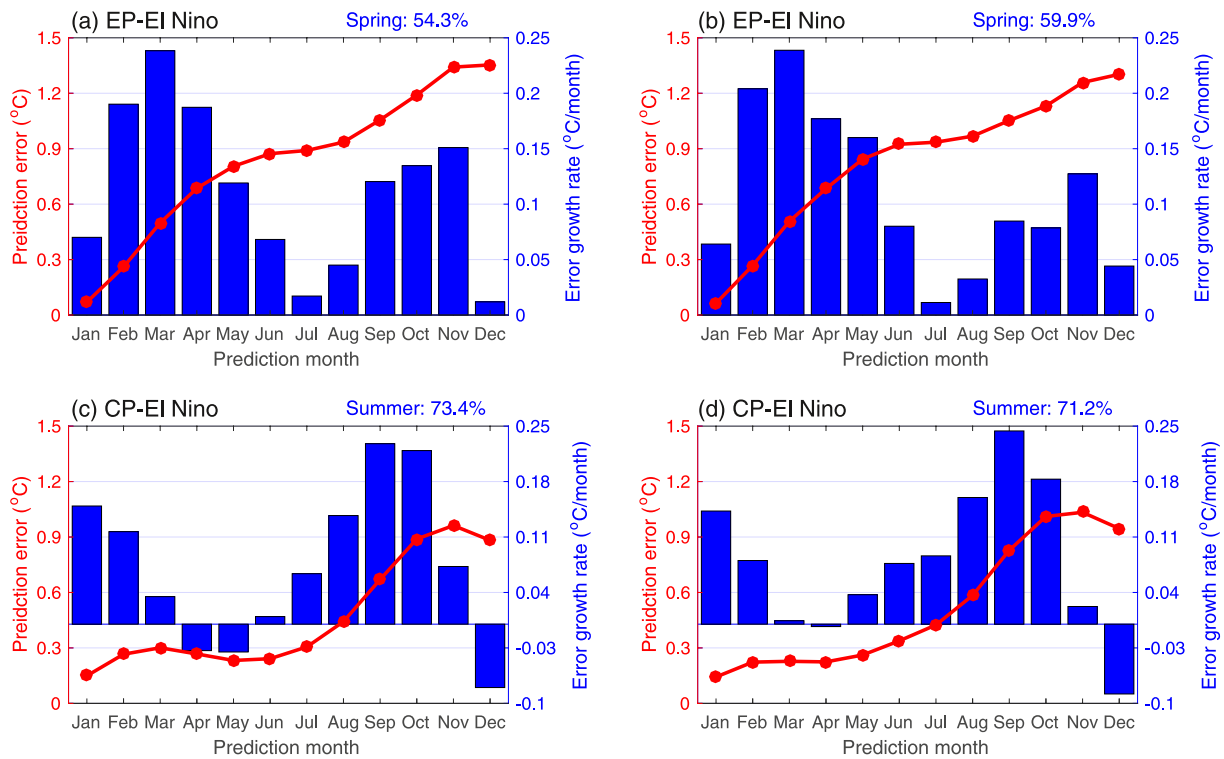
**Figure 2.** Horizontal distributions of two types of CNOP-U with the greatest impact on El Niño predictions. The contour interval is 0.25 m/s.

As shown in Figure 2, the first type of CNOP-U (denoted as type-1 CNOP-U) features a positive value in the western and central tropical Pacific, whereas the second type of CNOP-U (denoted as type-2 CNOP-U) has a similar horizontal distribution but an opposite phase. The details are different (Figure S2 in Supporting Information S1). For example, one can find that the type-1 CNOP-U is mainly located over the regions in the north equatorial countercurrent and south equatorial current near the dateline. In contrast, the type-2 CNOP-U has a broader latitudinal range that extends 140°W more to the east than that of the type-1 CNOP-U.

Figures 3a and 3b shows the prediction errors in the SST anomaly at the end of the El Niño prediction when these CNOP-Us are added into the initial ZC. The SST prediction errors are positive (up to 2°C) in the eastern tropical Pacific at the end of prediction when the type-1 CNOP-U exists in the initial condition, while they are negative (up to -2°C) when the type-2 CNOP-U exists in the initial condition. That is, the type-1 and type-2 CNOP-Us tend to cause EP El Niño-like error and EP La Niña-like error, respectively. However, the impacts of the type-1 or type-2 CNOP-Us on the growth of prediction errors are dependent on the type of El Niño events. On the one hand, the CNOP-U can induce a larger prediction error in the CP El Niño prediction than in the EP El Niño prediction, as indicated by the object function (Table S1 in Supporting Information S1). This result illustrates that the prediction of CP El Niño is more sensitive to the initial ZC than that of EP El Niño. On the other hand, by focusing on the horizontal distribution of the prediction errors, we can find that the main difference in



**Figure 3.** Prediction errors in the sea surface temperature (SST) anomalies induced by the (a) type-1 and (b) type-2 CNOP-Us. Differences in the prediction errors between the eastern Pacific (EP) and central Pacific (CP) El Niño predictions induced by the (c) type-1 and (d) type-2 CNOP-Us. The contour interval in (a) and (b) is 0.5°C, whereas that in (c) and (d) is 0.2°C.



**Figure 4.** (Red curves) Prediction errors and (blue bars) growth rates in the eastern Pacific (EP) and central Pacific (CP) El Niño predictions. The left panels indicate errors induced by the type-1 CNOP-U, and the right panels indicate those induced by the type-2 CNOP-U. The number at the top right-hand corner of each panel denotes the ratio of the error growth in spring or summer to the total error growth, which quantifies the PB strength.

the errors between the EP and CP El Niño predictions exists in the central tropical Pacific (Figures 3c and 3d). Specially, the type-1 CNOP-U tends to induce larger positive errors in the central tropical Pacific in the CP El Niño prediction than in the EP El Niño prediction. The type-2 CNOP-U has a colder effect on the central tropical Pacific during the CP El Niño than during the EP El Niño prediction. Thus, the model with the type-1 CNOP-U can predict a stronger-than-observed El Niño event. The model with the type-2 CNOP-U can predict a weaker El Niño event when an EP El Niño event actually occurs but tend to predict a normal or even a cooling event when a CP El Niño event actually occurs as the amplitude of the CP El Niño is usually less than 1.5°C (Figure S1 in Supporting Information S1).

Next, we investigate the temporal evolution of the SST prediction errors from the start month to the end month. To quantify the uncertainties in the amplitude prediction of the two types of El Niño events, the prediction error at time  $t$  ( $E_t$ ) is defined as

$$E_t = \frac{1}{N} \sum_{i,j} (T'_{i,j,t} - T_{i,j,t})^2 \quad (6)$$

where  $T'_{i,j,t}$  and  $T_{i,j,t}$  are the predicted and reference SST anomalies in the model grid ( $i,j$ ), respectively, and  $N$  is the number of model grids in a certain region. One factor that we need to highlight is that the EP and CP El Niño peak in the central and eastern tropical Pacific, respectively. Thus, for the EP and CP El Niño predictions, the prediction errors are calculated over the Niño3 and Niño4 regions using Equation 6, respectively. The error growth rate is defined as  $\tau_t = E_t - E_{t-1}$ .

The prediction errors and growth rates induced by the CNOP-Us are shown in Figure 4. We can observe that the prediction errors increase over time; however, the growth rate is dependent on the calendar month. Moreover, the CNOP-U-induced SST error evolutions in the EP and CP El Niño predictions are different. For example, in the EP El Niño prediction (Figure 4a), the prediction error induced by the type-1 CNOP-U grows fastest in spring (February to May) in the whole year. The prediction error of the CP El Niño event that is caused by the type-1 CNOP-U is also critically dependent on time but exhibits the highest growth rate in

summer (July to October). Looking at the error growth induced by the type-2 CNOP-U, the maximum error growth rates in the EP and CP El Niño also occur in spring and summer, respectively. Such seasonally dependent error growth is known as the PB phenomenon. In Section 1, we presented the review of the predictability of the CP and EP El Niño and mentioned that the EP El Niño prediction suffers from spring PB while the CP El Niño prediction suffers from summer PB. According to the results shown in Figure 4, the spring or summer PB might have been caused in part by the initial errors in the ZC. Specifically, the CNOP type of ZC error that is mainly located in the central and western tropical Pacific is one of the factors that lead to the occurrence of the PB phenomenon.

To quantify the PB strength induced by the ZC uncertainties, we calculate the ratio of the error growth in one definite season to the total error growth for the whole year. It can be found that the strength of summer PB in the CP El Niño prediction is greater than that of spring PB during the EP El Niño prediction (top right-hand corner in each panel in Figure 4). The error growth in summer accounts for more than 70% of the total error growth in the CP El Niño prediction. It is implied that the initial ZC errors in the central tropical Pacific can cause fast error growth in summer during the CP El Niño prediction. From this point, reducing the initial ZC errors in the western tropical Pacific may be effective in dissipating summer PB and is thus favored to enhance the CP El Niño prediction.

To further verify the above conjecture, several sensitivity experiments are made (see Text S1 in Supporting Information S1). The ZC errors existed in the central and western tropical Pacific can account for more than 50% of the total error growth that are induced by the CNOP-U (Figures S3 and S4 in Supporting Information S1). Moreover, the spring PB in EP El Niño prediction and summer PB in CP El Niño become much more serious when ZC errors only exist in the central and western tropical Pacific. The result demonstrates further demonstrate that reducing the initial ZC errors in the western and central tropical Pacific is vital in weakening the PB phenomena and reducing the prediction uncertainties for both EP and CP El Niño predictions.

#### 4. Dynamics of the Seasonal-Dependent Error Growth Induced by CNOP-Us

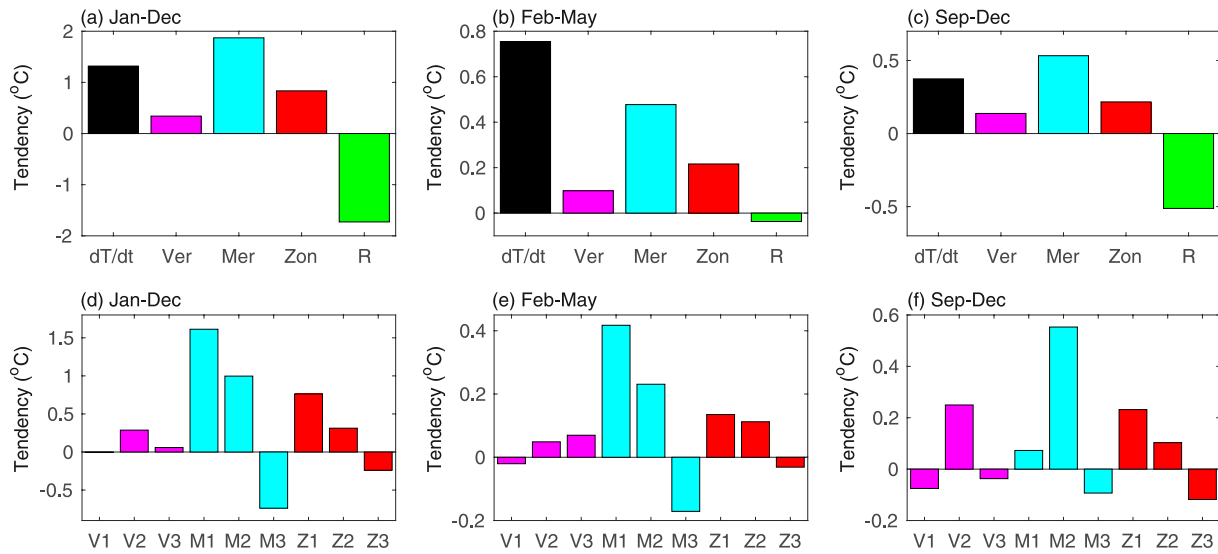
The last section states that the largest-growing types of initial ZC errors do not depend on the type of El Niño, but their effects on the prediction error growth do. Specifically, the CNOP-Us tend to induce spring and summer PB-like error growth to the EP and CP El Niño predictions, respectively, which naturally leads to the question of why the CNOP-Us play different roles in the error growth in various El Niño predictions. Therefore, we intend to examine the mechanisms of the error growths in spring and summer and try to figure out the reasons why the timings of PB are linked to the type of El Niño. The results are presented in this section.

To accordingly investigate the dynamics that explain the spring and summer error growths of the EP and CP El Niño predictions, a heat budget analysis is performed over the Niño3 and Niño4 regions, respectively. According to Equations 4 and 5, the governing equation of the SST error evolution can be expressed as

$$\begin{aligned} \frac{\partial T^*}{\partial t} = & -u^* \frac{\partial \bar{T}}{\partial x} - \bar{u} \frac{\partial T^*}{\partial x} - \left( u^* \frac{\partial T^*}{\partial x} + u^* \frac{\partial T'}{\partial x} + u' \frac{\partial T^*}{\partial x} \right) \\ & -v^* \frac{\partial \bar{T}}{\partial y} - \bar{v} \frac{\partial T^*}{\partial y} - \left( v^* \frac{\partial T^*}{\partial y} + v^* \frac{\partial T'}{\partial y} + v' \frac{\partial T^*}{\partial y} \right) \\ & -w^* \frac{\partial \bar{T}}{\partial z} - \bar{w} \frac{\partial T^*}{\partial z} - \left( w^* \frac{\partial T^*}{\partial z} + w^* \frac{\partial T'}{\partial z} + w' \frac{\partial T^*}{\partial z} \right) \\ & + R^* \end{aligned} \quad (7)$$

where  $T^*$ ,  $(u^*, v^*, w^*)$ , and  $R^*$  are the errors in the SST, ocean currents, and residual term (i.e., HF + DF), respectively, that are caused by the CNOP-Us. We can observe that the tendency of the SST errors is governed by the linear ocean advection terms (e.g.,  $-u^* \frac{\partial \bar{T}}{\partial x}$  and  $-\bar{u} \frac{\partial T^*}{\partial x}$ ) and nonlinear terms (e.g.,  $u^* \frac{\partial T^*}{\partial x} + u^* \frac{\partial T'}{\partial x} + u' \frac{\partial T^*}{\partial x}$ ). For convenience, the zonal advection of the mean SST by the ZC error, SST error by the mean ZC, and the nonlinear terms are denoted as Z1, Z2, and Z3, the meridional ones as M1, M2, and M3, and vertical advection ones as V1, V2, and V3, respectively. By comparing these terms, we can determine the key process that causes the seasonal error growth in the El Niño prediction.





**Figure 5.** Heat budget terms of the error evolution over the Niño3 region induced by type-1 CNOP-U in the eastern Pacific (EP) El Niño prediction. The results are obtained from six ensembles of EP El Niño predictions. The left, middle, and right panels show the calculation using Equation 7 during the whole year, spring (February to May), and fall (September to December), respectively. The heat budget terms along the x-axis in (a–c) indicate the sea surface temperature (SST) anomaly tendency, vertical convection, meridional advection, zonal advection, and residual (diffusion and heat-flux) terms. The detailed heat transports by the ocean current are shown in (d–f). V1, V2, and V3 denote the vertical advection of the mean SST by the upwelling error ( $-w^* \frac{\partial T^*}{\partial z}$ ), that of the SST error by the mean upwelling ( $-\bar{w} \frac{\partial T^*}{\partial z}$ ), and that of the nonlinear terms [ $-(w^* \frac{\partial T^*}{\partial z} + w^* \frac{\partial T^*}{\partial z} + w' \frac{\partial T^*}{\partial z})$ ], respectively, and so are the meridional (M1, M2, and M3) and zonal-advection terms (Z1, Z2, and Z3). Z1 represents the zonal advection feedback, and V2 represents the thermocline feedback.

#### 4.1. Mechanisms of the Error Growth in Spring in the EP El Niño Prediction

Figure 5 shows the heat budget for the error evolution due to the type-1 CNOP-U in the EP El Niño prediction. Overall, the horizontal and vertical advectons positively contribute to the error growth (Figure 5a). In particular, the meridional advection is the dominant process, followed by the zonal advection. If these advection processes are further decomposed, we can observe that M1, M2, and Z1 contribute the most [Figure 5d]. This result reveals that the initial errors in the ZC over the western and central tropical Pacific (i.e., type-1 CNOP-U) tend to influence predictions of the meridional and zonal currents and result in large uncertainties in the horizontal advection, thus causing large SST error growth in the eastern tropical Pacific.

Comparing Figure 5a (Figure 5d) with Figure 5b (Figure 5e), one can find that the distribution of the heat budget in spring is identical to that in the whole year. The horizontal and vertical advectons is the main factor leading to the spring error growth, where the leading terms are the linear meridional advection and zonal advection feedback term ( $-u^* \frac{\partial T^*}{\partial x}$ ). Specifically, the tendency of the SST error in spring is approximately 0.75°C, whereas M1 ( $-v^* \frac{\partial T^*}{\partial y}$ ) is larger than 0.4°C. Therefore, we propose that the uncertainties in the meridional current caused by the type-1 CNOP-U are the factor that is responsible for inducing the spring PB phenomenon and final error growth in the EP El Niño prediction.

Because a second strong error growth rate is observed to occur from September to December (Figure 4), we also look at the heat budget during this period (Figures 5c and 5f). The tendency of the SST error from September to December is found to be much smaller than that in spring. Moreover, the roles of ocean processes are also different. From September to December, M2 ( $-\bar{v} \frac{\partial T^*}{\partial y}$ ) turns into a dominant process, which is the leading factor that accounts for the error growth, while V2 ( $-\bar{w} \frac{\partial T^*}{\partial z}$ ) is the second. In other words, at the end of the prediction of the EP El Niño event, climatological upwelling and the meridional current promote the growth of the SST error. By comparing the heat budget in spring and from September to December, we conclude that the seasonally dependent error growth results from the time-dependent ocean processes.

The heat budget related to the type-2 CNOP-U is shown in Figure 6. The involved mechanism that is responsible for the error growth is similar to the error dynamics induced by the type-1 CNOP-U, although the former causes a negative error growth. For example, the negative tendency of the SST error is strongly related to the negative

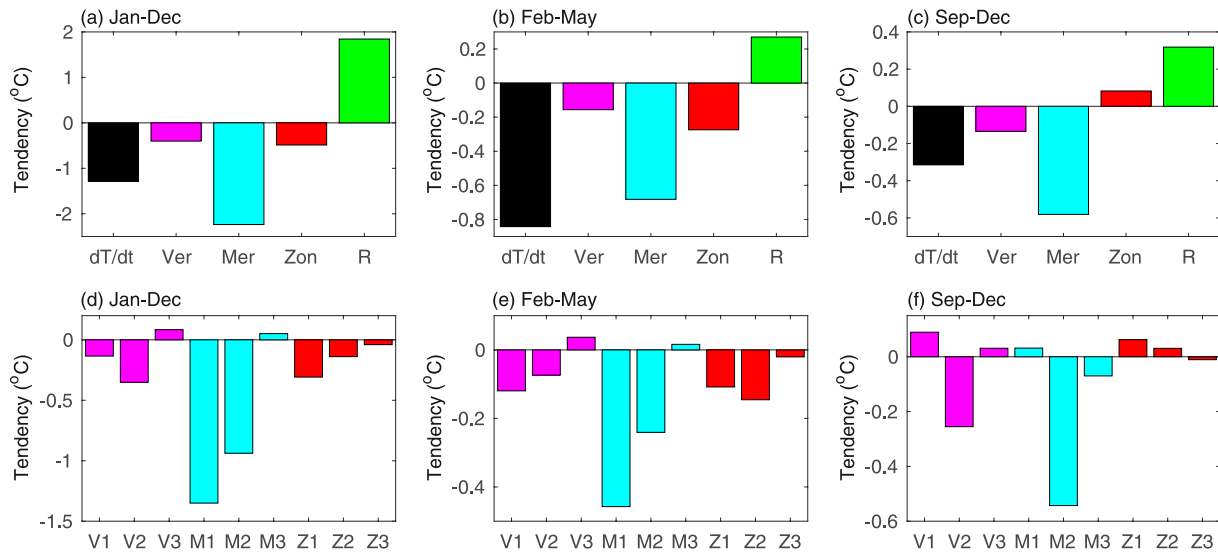


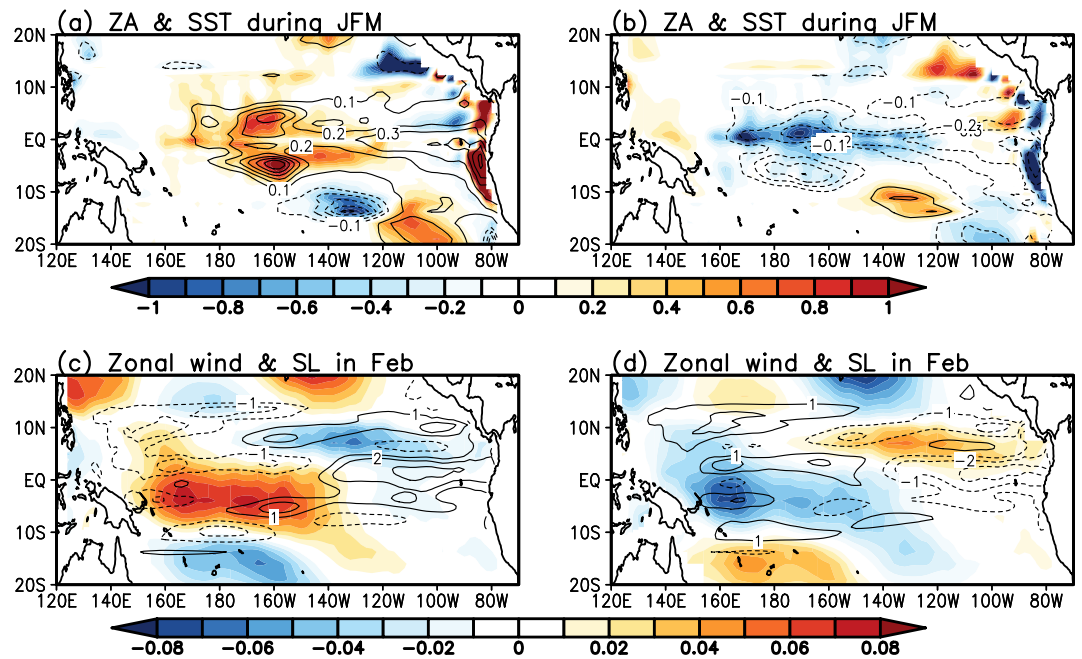
Figure 6. Similar to Figure 5 but induced by the type-2 CNOP-U.

tendency in the spring; the spring error growth is mostly contributed by the  $M1$  and  $M2$  terms. The contribution of  $Z2$  is greater than that of  $Z1$  in the error growth induced by type-2 CNOP, which differs from the case of type-1 CNOP. In other words, the magnitudes of contributions from  $Z1$  and  $Z2$  are reversed between the two cases.

Beyond that, one can find that the residual term  $R$  shows comparable magnitude even the larger magnitude in some cases compared with the advection terms. So, the undeniable fact is that the HF and DF do play roles in the SST tendency. However, the term  $R$  tends to show opposite sign against the SST tendency error, which indicates that the residual term  $R$  acts to hinder the SST error growth. Hence, the error growth during spring is the result of the ocean advection not the HF and DF terms.

According to the above analyses, the strong error growth in spring due to either type-1 or type-2 CNOP-U is mainly related to the errors in the meridional current in the eastern tropical Pacific. Because the CNOP-Us are mainly located in the western and central tropical Pacific, we might ask how the initial ZC errors lead to prediction errors in the meridional current in the eastern tropical Pacific. To answer this issue, we need to look back to see what changes have occurred in the ocean and atmosphere in the prediction period of the EP El Niño.

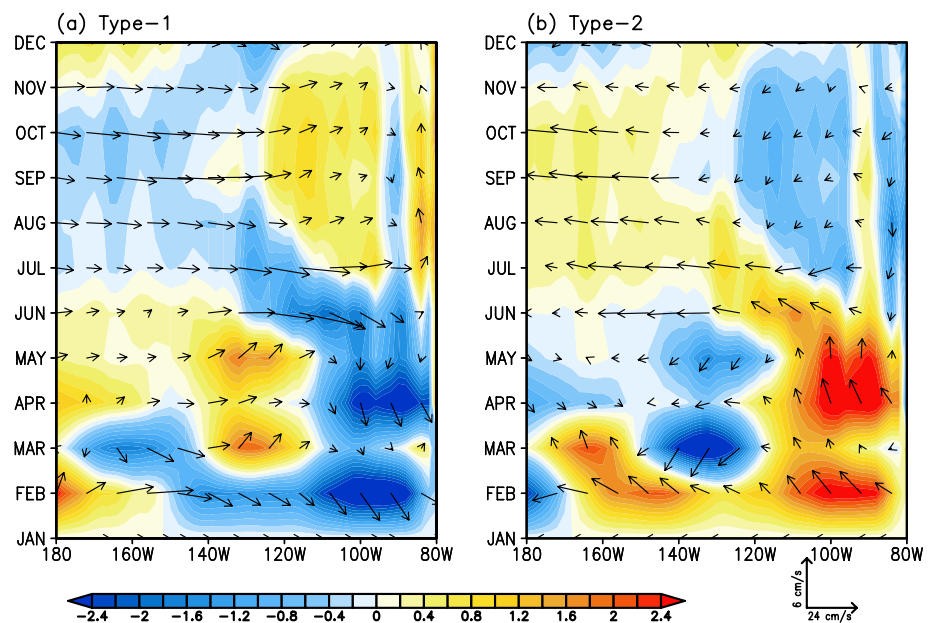
The changes in the ocean and atmosphere caused by the CNOP-Us are shown in Figures 7 and 8. We can observe that a significant SST error first occurs in the central tropical Pacific, whose horizontal pattern is quite similar to the errors in the zonal advection feedback (i.e.,  $Z1$ ,  $-u^* \frac{\partial \bar{T}}{\partial x}$ ). For example, the type-1 CNOP-U-induced positive SST errors from January to March are concentrated at the sides of the equator near  $160^\circ\text{W}$ , where changes in the zonal advection feedback peak with positive values. The similarity is understandable because the type-1 CNOP-U, with the largest positive values in the central tropical Pacific, can directly enhance the zonal advection feedback and warm up the ocean in these regions. Meanwhile, the type-1 CNOP-U triggers a stronger-than-the-reference westerly anomaly over the south of the central equatorial Pacific (centered at  $5^\circ\text{S}$ ) and a stronger-than-the-reference SL anomaly in the eastern tropical Pacific. The air-sea condition is conducive to enhancing the eastward current along the equator and cross-equatorial current from north to south in the eastern tropical Pacific (Figure 8a). Moreover, the enhanced cross-equatorial currents in the eastern tropical Pacific prevail during spring but rapidly weaken after June. For the spring predictions involving the type-2 CNOP-U, the errors in SST with negative values are also controlled by the weakened zonal advection feedback in the central tropical Pacific (Figure 7b). The westerly is therefore reduced together with the negative errors in SL in the eastern equatorial Pacific, which forces the ocean to enhance the northwestward current along the equator (Figure 8b). However, as the wind errors are enhanced enough by the air-sea coupling, the strengthened wind errors can trigger strong eastward Kelvin waves that are represented by symmetric sea level anomaly to hinder the cross-equatorial current error. The cross-equatorial current is thus gradually weakened after spring. Hence, the changes in the meridional currents in the eastern equatorial Pacific are shown to be dependent on time, with the largest values occurring in spring. It is



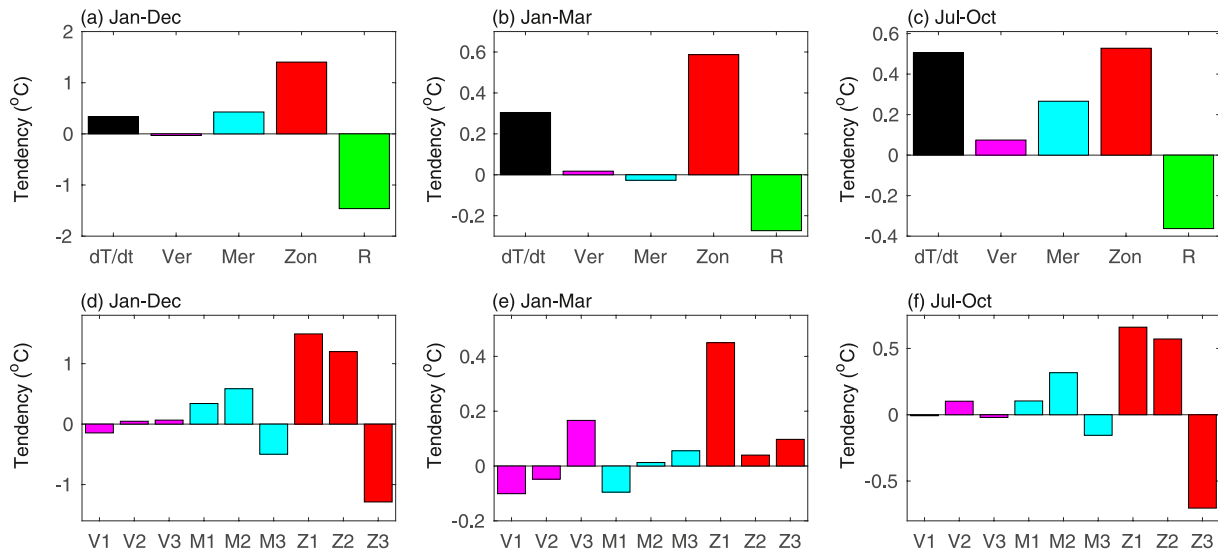
**Figure 7.** Changes in the (shaded) zonal advection feedback term and (contoured) sea surface temperature (SST) during January to March induced by (a) type-1 and (b) type-2 CNOP-Us in the eastern Pacific (EP) El Niño prediction. Changes in the (shaded) zonal wind stress and (contoured) sea level (SL) in February induced by (c) type-1 and (d) type-2 CNOP-Us in the EP El Niño prediction. The contour intervals are  $0.1^{\circ}\text{C}$  in (a and b) and  $1\text{ cm}$  in (c and d). Units of the color bars at the top and bottom panels are  $^{\circ}\text{C}$  and  $\text{dyn cm}^{-2}$ , respectively.

the reason why *M1* shows a seasonal dependence with the largest value occurring in spring and leading to a spring PB-like error growth in the EP El Niño prediction when the type-1 or type-2 CNOP-U exists in the initial condition.

Based on the abovementioned discussion, the main mechanism that explains the strong error growth in spring can be concluded as follows. When a type-1 (type-2) CNOP-U exists in the EP El Niño prediction, the positive



**Figure 8.** Changes in the (vectors) ocean current and (shading) cross-equatorial current along the equator caused by (a) type-1 and (b) type-2 CNOP-Us in the eastern Pacific El Niño prediction.



**Figure 9.** Heat-budget terms in the error evolution over the Niño4 region induced by type-1 CNOP-U in the central Pacific El Niño prediction.

(negative) ZC errors in the western and central tropical Pacific can enhance (reduce) the zonal-advection feedback and warm up (cool down) the central tropical ocean. Changes in the SST anomaly then influence the atmosphere on a basin-scale through the air–sea coupling and strengthen (weaken) the westerly over the central tropical Pacific. Because of the zonal wind anomaly, the ocean converges (diverges) in the eastern tropical Pacific, thus leading to a strong southeastward (northwestward) change in the cross-equatorial current during spring in the eastern tropical Pacific. The SST error rapidly increases during spring due to the meridional advection feedback ( $-v^* \frac{\partial T}{\partial y}$ ),  $t$ . Subsequently, the growth rate of the SST errors gradually decreases with the fading of the meridional current errors. Hence, PB of the EP El Niño prediction caused by the error in the ZC occurs in spring but not in other seasons.

#### 4.2. Mechanisms of Error Growth in Summer in the CP El Niño Prediction

The temporal evolution of the prediction errors and the dynamics of the seasonally dependent error growth in the CP El Niño are different from those in the EP El Niño. To quantify the processes involving the summer PB-associated error growth (similar to that discussed in Section 4.1), we also obtain the changes in each term of the heat budgets that are caused by the CNOP-Us in the CP El Niño prediction. The results related to the type-1 and type-2 CNOP-Us are shown in Figures 9 and 10, respectively.

For the prediction caused by the type-1 CNOP-U, Figure 9a shows that the horizontal advection exhibits positive contribution to the error growth, whereas the  $R$  term (diffusion and heat-flux terms) tends to inhibit the error growth in the whole prediction period. In particular, the zonal advection is found to be the main positive process, while the meridional advection is the second. Evidently, this result is different from the case of the EP El Niño prediction, where the contribution of the meridional advection is greater than that of the zonal advection. When these advection terms are decomposed, we can find that Z1 ( $-u^* \frac{\partial T}{\partial x}$ ) and Z2 ( $-\bar{u} \frac{\partial T^*}{\partial x}$ ) are the main processes that cause the positive error growth in the central tropical Pacific in the whole year.

The contribution of each term is dependent on the seasons. According to the time-dependent error growth rate (Figures 4c and 4d), the prediction error grows fast in the early prediction time and summer. Therefore, the heat budget terms in winter (from January to March) and summer (from July to October) are calculated respectively. It can be found that the zonal advection of the climatological SST by the ZC error ( $-u^* \frac{\partial T}{\partial x}$ ) plays a dominant role in the tendency of the SST error in the early time prediction (Figures 9b and 9e). This result is comprehensible because the type-1 CNOP-U with large positive values is located in the central tropical Pacific (Figure 2). In summer, Z2 and M2, along with Z1, exhibit a warming effect on the SST prediction. Moreover, the distributions

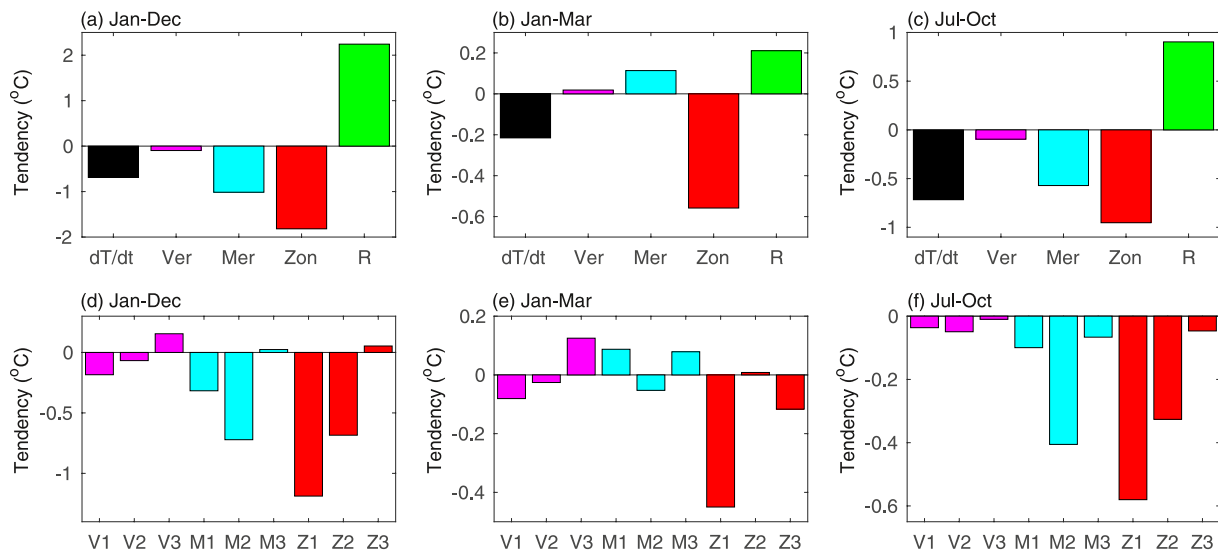


Figure 10. Similar to Figure 9 but induced by type-2 CNOP-U.

of the heat budget terms in summer are quite similar to those over the whole prediction period, indicating that the ocean processes in summer are primarily responsible for the emergence of the final prediction error.

Comparison and analysis of Figures 9 and 10 reveal that the mechanisms involved with the type-2 CNOP-U are identical to those of the type-1 CNOP-U. The error growth in summer is related to the strong cooling roles played by Z1 and Z2. Next, we figure out how the CNOP-U's cause changes in the linear zonal advection, consequently leading to a summer PB-like error evolution.

Figure 11 shows the changes in the SST tendency and zonal advection feedback in summer caused by the CNOP-U's. Their horizontal distributions are almost the same in which both the zonal advection feedback and SST tendency exhibit positive values in the central tropical Pacific in the type-1 CNOP-U case and negative values in the type-2 CNOP-U case. It means that the distribution of the SST error growth in summer is controlled by the ZC errors in the central tropical Pacific. Thus, the zonal gradient of the SST error ( $\frac{\partial T^*}{\partial x}$ ) is prominent in the Niño4 region and enhances the SST error growth in summer by the linear zonal advection of the mean current ( $-\bar{u} \frac{\partial T^*}{\partial x}$ ).

Focusing on the central tropical Pacific, the temporal changes in the oceanic and atmospheric variables in the CP El Niño predictions are shown in Figure 12. Figure 12a shows that under the influence of the high values of the type-1 CNOP-U in the initial conditions, the predicted eastward currents in the central tropical Pacific are stronger than the reference in the early months of the year. Later, the positive ZC errors quickly decrease over time and are almost gone in April. The model with a stronger zonal advection feedback, therefore, tends to describe a warmer central tropical Pacific ocean. After April, the eastward ZC errors appear again and gradually increase until peak in summer. From the perspective of the atmosphere, the westerly errors

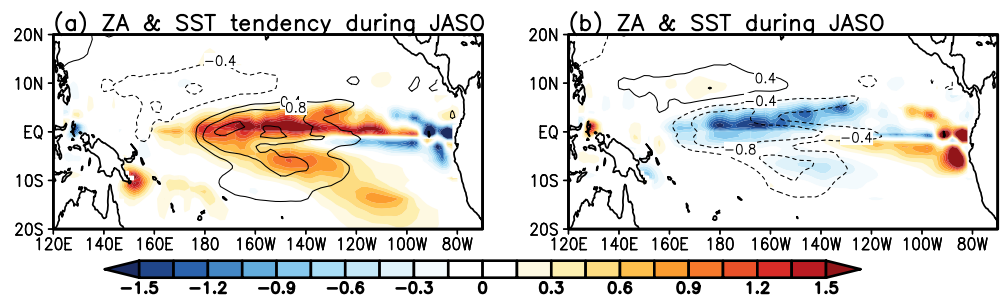
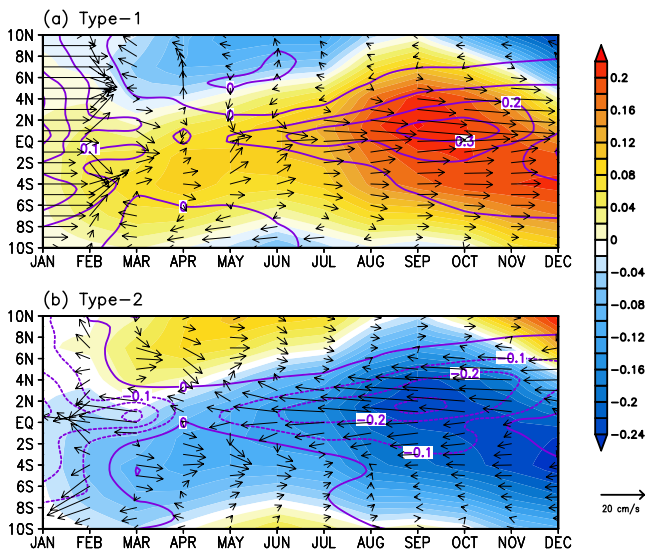


Figure 11. Changes in the (contoured) zonal advection feedback and (shaded) sea surface temperature (SST) tendency in summer induced by the (a) type-1 and (b) type-2 CNOP-U's in the central Pacific (CP) El Niño prediction. The contour interval is 0.4°C. The unit of the shading is °C.





**Figure 12.** Changes in the (vectors) ocean current, (contoured) zonal-advection feedback, and (shaded) zonal wind stress over the central tropical Pacific (averaged between 180°W and 120°W) caused by the (a) type-1 and (b) type-2 CNOP-Us in the central Pacific (CP) El Niño prediction as a function of time and latitude. The units of the ocean current and wind stress are cm/s and  $\text{dyn cm}^{-2}$ , respectively. The contour interval is  $0.1^\circ\text{C}/\text{month}$ .

first appear over the south of the central tropical Pacific, which gradually shift to the equator and peak in summer. Figure 12b shows the case of the type-2 CNOP-U. The error evolutions of the air and sea are identical to those of the type-1 CNOP-U case but with an opposite sign. Generally, during the CP El Niño prediction, the type-1 or type-2 CNOP-U can induce strong air-sea coupling uncertainties in summer with the largest errors in both zonal wind and ZC, thus leading to the summer PB-associated error growth.

The above results indicate that the CNOP-U can trigger seasonally dependent ocean processes thus causing the summer PB-like error growth during the CP El Niño prediction. The involved mechanisms are concluded to be the following. When the type-1 (type-2) CNOP-U is present in the initial condition in the CP El Niño prediction, the positive (negative) ZC errors in the western and central tropical Pacific tend to warm up (cool down) the central tropical ocean due to the enhanced (reduced) zonal advection feedback. Subsequently, the kinetic energy of the ZC errors quickly disperses in the early year. While, triggered by the positive (negative) SST errors, the westerly (easterly) errors appear which in turn provide the potential to enhance the eastward (westward) current. Under the air-sea coupling, the zonal wind errors continuously increase and shift to the equator acting to re-generate and enhance the ZC errors. Such air-sea coupling uncertainties peak in summer. Therefore, the prediction errors rapidly increase in summer due to the CNOP-U-induced great changes in the linear zonal advection ( $-u^* \frac{\partial T}{\partial x}$  and  $-\bar{u} \frac{\partial T^*}{\partial x}$ ) in the CP El Niño prediction.

## 5. Summary and Discussion

The dominant dynamics regarding the EP and CP El Niño vary in the tropical Pacific. For instance, previous studies emphasized the distinct important roles of the thermocline and zonal advection feedback in the developments of the EP and CP El Niño. Many efforts are thus made to explore the ENSO predictability related to the initial uncertainties in ocean temperature (e.g., Duan & Hu, 2016; Hou et al., 2019; Tao et al., 2017). However, few studies investigate the relationship between the prediction and initial errors in the ZC. Therefore, from the perspective of error growth, the present study investigates the predictability of two types of El Niño in terms of the initial ZC effects. Based on the CNOP approach, the CNOP-Us that can induce the largest error growth in the El Niño predictions are revealed using a pre-corrected ENSO model (NFSV-ICM). Two types of CNOP-Us are identified that exhibit similar horizontal patterns but with opposite signs. The type-1 CNOP-U features large positive values over the regions in the north equatorial countercurrent and south equatorial current near the dateline. The type-2 CNOP-U exhibits large negative values in the western and central tropical Pacific.

The impacts of the CNOP-Us on the predictions of the different types of El Niño events vary accordingly. For example, the type-1 CNOP-U tends to induce El Niño-like error evolution, but the induced positive SST errors in the CP El Niño prediction are larger than those in the EP El Niño prediction. The differences are most obvious in the central tropical Pacific. When a type-2 CNOP-U is present in the initial conditions of the model, the induced SST errors in the CP El Niño prediction are also greater than those in the EP El Niño prediction. In particular, the type-2 CNOP-U can cause larger negative SST errors in the central tropical Pacific. The CP El Niño prediction is implied to be more sensitive to the initial ZC than the EP El Niño prediction, which is also consistent with the previous studies that suggest the greater importance of the zonal advection in the CP El Niño than in the EP El Niño evolutions (Kug et al., 2009; Yu et al., 2010).

The CNOP-U-induced temporal error growths between the EP and CP El Niño predictions are also different. The CNOP-Us cause the largest error growth rate in spring in the EP El Niño prediction and in summer in the CP El Niño prediction, which means that the CNOP-type initial error in the ZC is one of the sources of spring PB in the EP El Niño and summer PB in the CP El Niño. In addition, the strength of the induced PB in the CP El Niño prediction is much greater than that in the EP El Niño prediction. This result is also reflected in the fact that the predictability of CP El Niño is closely related to uncertainties in the ZC.

Heat budget analyses on the error evolution are implemented to quantify the main processes that explain the seasonal error growth. With regard to the prediction of the EP El Niño event, the strong growth in the SST error in spring is mainly controlled by the meridional advection of the mean SST by the meridional current error ( $-v^* \frac{\partial \bar{T}}{\partial y}$ ) induced by the CNOP-U<sub>s</sub>. Due to the strong effect of  $-v^* \frac{\partial \bar{T}}{\partial y}$  in spring, the total growth of the SST error is also related to the uncertainties in the meridional heat transport. Evidently, the change in the meridional current induced by the CNOP-U<sub>s</sub> is considered to be the responsible factor that causes the spring PB and final error growth in the EP El Niño prediction. The mechanisms of the spring PB-like error growth are revealed as follows. The strong initial errors in the ZC in the central and western tropical Pacific tend to increase the SST errors through the zonal advection feedback in the central tropical Pacific. The errors in the zonal wind and SL increase due to the air–sea interaction, thus affecting the cross-equatorial current and leading to large errors in the meridional current along the eastern equatorial Pacific in spring. The SST prediction errors in the eastern tropical Pacific, therefore, quickly increase in spring by the strong uncertainties in the meridional advection feedback. With the weakening of the meridional current errors, the growth of the SST error also slows down, thus leading to seasonal-dependent error growth for the EP El Niño prediction.

With regard to the prediction of the CP El Niño, errors in the SST tendency in summer are primarily dependent on the uncertainties in the linear zonal advection ( $-u^* \frac{\partial \bar{T}}{\partial x}$  and  $-\bar{u} \frac{\partial T^*}{\partial x}$ ). At the start of the prediction, errors in the ZC in the western and central tropical Pacific can change the zonal advection feedback and heavily impact the SST prediction in the region. Triggered by the SST errors, zonal wind errors appear, which in turn force the ocean to generate large ZC errors. Under the air–sea coupling, the zonal wind errors continuously increase and shift to the equator acting to enhance the ZC errors. Errors in the zonal wind and ZC reach their peak during summer, which leads to a fastest SST error growth in summer through the linear zonal advection processes. Therefore, the emergence of summer PB for CP El Niño prediction is partly caused by the errors in the ZC in the central and western tropical Pacific.

Because the CNOP-U represents the most unstable mode of initial errors in the El Niño prediction, the specific distributions of the CNOP-U<sub>s</sub> imply that the El Niño prediction is sensitive to the initial ZC in the western and central tropical Pacific. In fact, by developing an optimal regression model to predict the El Niño event based on historical observation, Wang et al. (2017) have identified that the ocean currents near the dateline and southern edge of the south equatorial current are an important precursor of El Niño events. From the error growth perspective, the present study also highlights the significance of the initial ZC in these regions for predicting EP and CP El Niño events. Given this, it is crucial to prioritize intensive observations of the ZC in the western and central tropical Pacific to improve the accuracy of El Niño predictions, particularly for CP El Niño events. This not only helps avoid the CNOP-type initial errors but also helps capture the precursor of El Niño. Thus, the PB phenomena can be further weakened to yield better predictions of El Niño diversity.

It should be noted that the conclusions drawn here are based on examining the potential impacts of the ZC errors in January on the EP and CP El Niño predictions. However, it's worth mentioning that the impacts of the initial errors on the predictions are not only restricted to the El Niño type alone but also related to the start time of the prediction. Further, it has been found that the CNOP-type of ZC errors varies with initial seasons, as demonstrated in Text S2 and Figures S5 and S6 in Supporting Information S1. This suggests that the initial error regions that have the greatest effect on El Niño predictions change over time. Therefore, a rational plan for the time-dependent observation network is necessary to reduce the influence of initial ZC errors and improve the prediction of El Niño diversity.

### Data Availability Statement

The SST datasets are obtained from the NOAA reconstructed SST data (ERSSTv5; Huang et al., 2017) that cover the period from 1854 to the present (downloaded at <https://doi.org/10.7289/V5T72FNM>). All scripts used to analyze the data and generate the figures are written using the GrADS 2.2.1 (Tsai & Doty, 1998; <http://cola.gmu.edu/grads/downloads.php>) software and MATLAB 2018b (Morel, 2018).

## Acknowledgments

We express our sincere gratitude to the anonymous reviewers for their constructive suggestions. This study was supported by the Ministry of Science and Technology of the People's Republic of China (Grant 2020YFA0608802), the China Postdoctoral Science Foundation (Grant 2020M681155), the Guangdong Major Project of Basic and Applied Basic Research (Grant 2020B0301030004). Zhang is supported by the National Natural Science Foundation of China (NSFC; Grant 42030410). Zhang and Tao are supported by the Startup Foundation for Introducing Talent of NUIST.

## References

- Alexander, M. A., Blade, I., Newman, M., Lanzante, J. R., Lau, N. C., & Scott, J. D. (2002). The atmospheric bridge: The influence of ENSO teleconnections on air-sea interaction over the global oceans. *Journal of Climate*, *15*(16), 2205–2231. [https://doi.org/10.1175/1520-0442\(2002\)015<2205:tabtio>2.0.co;2](https://doi.org/10.1175/1520-0442(2002)015<2205:tabtio>2.0.co;2)
- An, S. I., Jin, F. F., & Kang, I. S. (1999). The role of zonal advection feedback in phase transition and growth of ENSO in the Cane-Zebiak model. *Journal of the Meteorological Society of Japan*, *77*(6), 1151–1160. [https://doi.org/10.2151/jmsj1965.77.6\\_1151](https://doi.org/10.2151/jmsj1965.77.6_1151)
- Bjerknes, J. (1969). Atmospheric teleconnections from Equatorial Pacific. *Monthly Weather Review*, *97*(3), 163–172. [https://doi.org/10.1175/1520-0493\(1969\)097<003C163:atfep%003E2.3.co;2](https://doi.org/10.1175/1520-0493(1969)097<003C163:atfep%003E2.3.co;2)
- Chen, N., Fang, X. H., & Yu, J. Y. (2022). A multiscale model for El Niño complexity. *npj Climate and Atmospheric Science*, *5*(1), 16. <https://doi.org/10.1038/s41612-022-00241-x>
- Delcroix, T., Eldin, G., Radenac, M. H., Toole, J., & Firing, E. (1992). Variation of the Western equatorial Pacific-ocean, 1986–1988. *Journal of Geophysical Research*, *97*(C4), 5423–5445. <https://doi.org/10.1029/92jc00127>
- Duan, W., & Mu, M. (2018). Predictability of El Niño-Southern Oscillation events. *Oxford Research Encyclopedia of Climate Science*. <https://doi.org/10.1093/acrefore/9780190228620.013.80>
- Duan, W. S., & Hu, J. Y. (2016). The initial errors that induce a significant "spring predictability barrier" for El Niño events and their implications for target observation: Results from an earth system model. *Climate Dynamics*, *46*(11–12), 3599–3615. <https://doi.org/10.1007/s00382-015-2789-5>
- Duan, W. S., Li, X. Q., & Tian, B. (2018). Towards optimal observational array for dealing with challenges of El Niño-Southern Oscillation predictions due to diversities of El Niño. *Climate Dynamics*, *51*(9–10), 3351–3368. <https://doi.org/10.1007/s00382-018-4082-x>
- Duan, W. S., Tian, B., & Xu, H. (2014). Simulations of two types of El Niño events by an optimal forcing vector approach. *Climate Dynamics*, *43*(5–6), 1677–1692. <https://doi.org/10.1007/s00382-013-1993-4>
- Fang, X. H., & Mu, M. (2018). A three-region conceptual model for central Pacific El Niño including zonal advective feedback. *Journal of Climate*, *31*(13), 4965–4979. <https://doi.org/10.1175/jcli-d-17-0633.1>
- Fang, X. H., & Xie, R. (2020). A brief review of ENSO theories and prediction. *Science China Earth Sciences*, *63*(4), 476–491. <https://doi.org/10.1007/s11430-019-9539-0>
- Feng, J., Lian, T., Ying, J., Li, J. D., & Li, G. (2020). Do CMIP5 models show El Niño diversity? *Journal of Climate*, *33*(5), 1619–1641. <https://doi.org/10.1175/jcli-d-18-0854.1>
- Gao, C., Chen, M., Zhou, L., Feng, L., & Zhang, R. H. (2022). The 2020–21 prolonged La Niña evolution in the tropical Pacific. *Science China Earth Sciences*, *65*(12), 2248–2266. <https://doi.org/10.1007/s11430-022-9985-4>
- Gao, C., Wu, X., & Zhang, R. H. (2016). Testing four dimensional variational data assimilation method using an improved intermediate coupled model for ENSO analysis and prediction. *Advances in Atmospheric Sciences*, *33*(7), 875–888. <https://doi.org/10.1007/s00376-016-5249-1>
- Gao, C., Zhang, R. H., Wu, X., & Sun, J. (2018). Idealized experiments for optimizing model parameters using a 4D-Variational method in an intermediate coupled model of ENSO. *Advances in Atmospheric Sciences*, *35*, 410–422. <https://doi.org/10.1007/s00376-017-7109-z>
- Ham, Y. G., Kug, J. S., Park, J. Y., & Jin, F. F. (2013). Sea surface temperature in the north tropical Atlantic as a trigger for El Niño/Southern Oscillation events. *Nature Geoscience*, *6*(2), 112–116. <https://doi.org/10.1038/ngeo1686>
- Hou, M. Y., Duan, W. S., & Zhi, X. F. (2019). Season-dependent predictability barrier for two types of El Niño revealed by an approach to data analysis for predictability. *Climate Dynamics*, *53*(9–10), 5561–5581. <https://doi.org/10.1007/s00382-019-04888-w>
- Hou, M. Y., Tang, Y. M., Duan, W. S., & Shen, Z. Q. (2023). Toward an optimal observational array for improving two flavors of El Niño predictions in the whole Pacific. *Climate Dynamics*, *60*(3–4), 831–850. <https://doi.org/10.1007/s00382-022-06342-w>
- Hsin, Y. C., & Qiu, B. (2012). The impact of eastern-Pacific versus central-Pacific El Niños on the North Equatorial Countercurrent in the Pacific Ocean. *Journal of Geophysical Research*, *117*(C11). <https://doi.org/10.1029/2012jc008362>
- Huang, B., Thorne, P. W., Banzon, V. F., Boyer, T., Chepurin, G., Lawrimore, J. H., et al. (2017). Extended reconstructed sea surface temperature, Version 5 (ERSSTv5): Upgrades, validations, and intercomparisons [Dataset]. *Journal of Climate*, *30*, 8179–8205. <https://doi.org/10.1175/JCLI-D-16-0836.1>
- Jin, E. K., Kinter, J. L., Wang, B., Park, C. K., Kang, I. S., Kirtman, B. P., et al. (2008). Current status of ENSO prediction skill in coupled ocean-atmosphere models. *Climate Dynamics*, *31*(6), 647–664. <https://doi.org/10.1007/s00382-008-0397-3>
- Jin, F. F. (1997). An equatorial ocean recharge paradigm for ENSO. Part I: Conceptual model. *Journal of the Atmospheric Sciences*, *54*(7), 811–829. [https://doi.org/10.1175/1520-0469\(1997\)054<0811:aeropf>2.0.co;2](https://doi.org/10.1175/1520-0469(1997)054<0811:aeropf>2.0.co;2)
- Keenlyside, N., & Kleeman, R. (2002). Annual cycle of equatorial zonal currents in the Pacific. *Journal of Geophysical Research*, *107*(C8), 1–13. <https://doi.org/10.1029/2000JC000711>
- Keenlyside, N. S. (2001). *Improved modelling of zonal currents and SST in the tropical Pacific*. Monash University, Department of Mathematics and Statistics.
- Kim, W., & Cai, W. J. (2014). The importance of the eastward zonal current for generating extreme El Niño. *Climate Dynamics*, *42*(11–12), 3005–3014. <https://doi.org/10.1007/s00382-013-1792-y>
- Kug, J. S., Jin, F. F., & An, S. I. (2009). Two types of El Niño events: Cold tongue El Niño and warm pool El Niño. *Journal of Climate*, *22*, 1499–1515. <https://doi.org/10.1175/2008jcli2624.1>
- Lee, H. C., Kumar, A., & Wang, W. Q. (2018). Effects of ocean initial perturbation on developing phase of ENSO in a coupled seasonal prediction model. *Climate Dynamics*, *50*(5–6), 1747–1767. <https://doi.org/10.1007/s00382-017-3719-5>
- Levine, A. F. Z., & McPhaden, M. J. (2015). The annual cycle in ENSO growth rate as a cause of the spring predictability barrier. *Geophysical Research Letters*, *42*(12), 5034–5041. <https://doi.org/10.1002/2015gl064309>
- Liu, Z. Y., Jin, Y. S., & Rong, X. Y. (2019). A theory for the seasonal predictability barrier: Threshold, timing, and intensity. *Journal of Climate*, *32*(2), 423–443. <https://doi.org/10.1175/jcli-d-18-0383.1>
- McCreary, J. P. (1981). A linear stratified ocean model of the equatorial undercurrent. *Philosophical Transactions of the Royal Society A*, *298*, 603–635. <https://doi.org/10.1098/rsta.1981.0002>
- McPhaden, M. J. (2015). COMMENTARY: Playing hide and seek with El Niño. *Nature Climate Change*, *5*(9), 791–795. <https://doi.org/10.1038/nclimate2775>
- Moore, A. M., & Kleeman, R. (1996). The dynamics of error growth and predictability in a coupled model of ENSO. *The Quarterly Journal of the Royal Meteorological Society*, *122*(534), 1405–1446. <https://doi.org/10.1002/qj.49712253409>
- Morel, P. (2018). Gramm: Grammar of graphics plotting in MATLAB [Software]. *Journal of Open Source Software*, *3*, 568. <https://doi.org/10.21105/joss.00568>

- Mu, M., Duan, W. S., & Wang, B. (2003). Conditional nonlinear optimal perturbation and its applications. *Nonlinear Processes in Geophysics*, 10(6), 493–501. <https://doi.org/10.5194/npg-10-493-2003>
- Mu, M., Xu, H., & Duan, W. S. (2007). A kind of initial errors related to "spring predictability barrier" for El Niño events in Zebiak-Cane model. *Geophysical Research Letters*, 34(3), L03709. <https://doi.org/10.1029/2006gl027412>
- Philander, S. G. H. (1983). El-Niño Southern Oscillation phenomena. *Nature*, 302(5906), 295–301. <https://doi.org/10.1038/302295a0>
- Qi, Q. Q., Duan, W. S., & Xu, H. (2021). The most sensitive initial error modes modulating intensities of CP- and EP-El Niño events. *Dynamics of Atmospheres and Oceans*, 96, 101257. <https://doi.org/10.1016/j.dynatmoce.2021.101257>
- Ren, H. L., Jin, F. F., Tian, B., & Scaife, A. A. (2016). Distinct persistence barriers in two types of ENSO. *Geophysical Research Letters*, 43(20), 10973–10979. <https://doi.org/10.1002/2016gl071015>
- Ren, H. L., Scaife, A. A., Dunstone, N., Tian, B., Liu, Y., Ineson, S., et al. (2018). Seasonal predictability of winter ENSO types in operational dynamical model predictions. *Climate Dynamics*, 52(7–8), 3869–3890. <https://doi.org/10.1007/s00382-018-4366-1>
- Ren, H. L., Zuo, J. Q., & Deng, Y. (2018). Statistical predictability of Niño indices for two types of ENSO. *Climate Dynamics*, 52(9–10), 5361–5382. <https://doi.org/10.1007/s00382-018-4453-3>
- Tang, Y. M., Zhang, R. H., Liu, T., Duan, W., Yang, D., Zheng, F., et al. (2018). Progress in ENSO prediction and predictability study. *National Science Review*, 5(6), 826–839. <https://doi.org/10.1093/nsr/nwy105>
- Tao, L. J., & Duan, W. S. (2022). A novel precursory signal of the central Pacific El Niño event: Eastern Pacific cooling mode. *Climate Dynamics*, 59(9–10), 2599–2617. <https://doi.org/10.1007/s00382-022-06229-w>
- Tao, L. J., Duan, W. S., & Jiang, L. (2022). Model errors of an intermediate model and their effects on realistic predictions of El Niño diversity. *International Journal of Climatology*, 42(15), 7443–7464. <https://doi.org/10.1002/joc.7656>
- Tao, L. J., Gao, C., & Zhang, R. H. (2018). ENSO predictions in an intermediate coupled model influenced by removing initial condition errors in sensitive areas: A target observation perspective. *Advances in Atmospheric Sciences*, 35(7), 853–867. <https://doi.org/10.1007/s00376-017-7138-7>
- Tao, L. J., Zhang, R. H., & Gao, C. (2017). Initial error-induced optimal perturbations in ENSO predictions, as derived from an intermediate coupled model. *Advances in Atmospheric Sciences*, 34(6), 791–803. <https://doi.org/10.1007/s00376-017-6266-4>
- Tian, B., & Duan, W. S. (2016). Comparison of the initial errors most likely to cause a spring predictability barrier for two types of El Niño events. *Climate Dynamics*, 47(3–4), 779–792. <https://doi.org/10.1007/s00382-015-2870-0>
- Timmermann, A., An, S. I., Kug, J. S., Jin, F. F., Cai, W., Capotondi, A., et al. (2018). El Niño-Southern Oscillation complexity. *Nature*, 559(7715), 535–545. <https://doi.org/10.1038/s41586-018-0252-6>
- Torrence, C., & Webster, P. J. (1998). The annual cycle of persistence in the El Niño Southern Oscillation. *The Quarterly Journal of the Royal Meteorological Society*, 124(550), 1985–2004. <https://doi.org/10.1002/qj.49712455010>
- Tsai, P., & Doty, B. E. (1998). A prototype java interface for the grid analysis and display system (GrADS). [Software]. Fourteenth International Conference on Interactive Information and Processing Systems, Phoenix, AZ, 11–16. <http://cola.gmu.edu/grads/downloads.php>
- Wang, J. N., Lu, Y. Y., Wang, F., & Zhang, R. H. (2017). Surface current in "hotspot" serves as a new and effective precursor for El Niño prediction. *Scientific Reports*, 7(1), 166. <https://doi.org/10.1038/s41598-017-00244-2>
- Webster, P. J., & Yang, S. (1992). Monsoon and ENSO: Selectively interactive systems. *The Quarterly Journal of the Royal Meteorological Society*, 118(507), 877–926. <https://doi.org/10.1002/qj.49711850705>
- Wei, Y. T., Mu, M., Ren, H. L., & Fu, J. X. (2019). Conditional nonlinear optimal perturbations of moisture triggering primary MJO Initiation. *Geophysical Research Letters*, 46(6), 3492–3501. <https://doi.org/10.1029/2018gl081755>
- Wyrtki, K. (1975). Fluctuations of dynamic topography in Pacific Ocean. *Journal of Physical Oceanography*, 5(3), 450–459. [https://doi.org/10.1175/1520-0485\(1975\)005<0450:fotdi>2.0.co;2](https://doi.org/10.1175/1520-0485(1975)005<0450:fotdi>2.0.co;2)
- Yang, Z., Fang, X., & Mu, M. (2020). The optimal precursor of El Niño in the GFDL CM2p1 model. *Journal of Geophysical Research: Oceans*, 125(3). <https://doi.org/10.1029/2019jc015797>
- Yeh, S. W., Kug, J. S., Dewitte, B., Kwon, M. H., Kirtman, B. P., & Jin, F. F. (2009). El Niño in a changing climate. *Nature*, 461(7263), 511–514. <https://doi.org/10.1038/nature08316>
- Yu, J. Y., Kao, H. Y., & Lee, T. (2010). Subtropics-related interannual sea surface temperature variability in the central equatorial Pacific. *Journal of Climate*, 23(11), 2869–2884. <https://doi.org/10.1175/2010jcli3171.1>
- Yu, Y. S., Duan, W. S., Xu, H., & Mu, M. (2009). Dynamics of nonlinear error growth and season-dependent predictability of El Niño events in the Zebiak-Cane model. *The Quarterly Journal of the Royal Meteorological Society*, 135(645), 2146–2160. <https://doi.org/10.1002/qj.526>
- Zebiak, S. E., & Cane, M. A. (1987). A model El-Niño Southern Oscillation. *Monthly Weather Review*, 115(10), 2262–2278. [https://doi.org/10.1175/1520-0493\(1987\)115%3c2262:AMENO%3e2.0.CO;2](https://doi.org/10.1175/1520-0493(1987)115%3c2262:AMENO%3e2.0.CO;2)
- Zhang, R. H., & Gao, C. (2016). The IOCAS intermediate coupled model (IOCAS ICM) and its real-time predictions of the 2015–2016 El Niño event. *Science Bulletin*, 61(13), 1061–1070. <https://doi.org/10.1007/s11434-016-1064-4>
- Zhang, R. H., Gao, C., & Feng, L. C. (2022). Recent ENSO evolution and its real-time prediction challenges. *National Science Review*, 9(4). <https://doi.org/10.1093/nsr/nwac052>
- Zhang, R. H., Zebiak, S. E., Kleeman, R., & Keenlyside, N. (2003). A new intermediate coupled model for El Niño simulation and prediction. *Geophysical Research Letters*, 30(19), 2012. <https://doi.org/10.1029/2003GL0181010>
- Zheng, F., Fang, X. H., Zhu, J., Yu, J. Y., & Li, X. C. (2016). Modulation of Bjerknes feedback on the decadal variations in ENSO predictability. *Geophysical Research Letters*, 43(24), 12560–12568. <https://doi.org/10.1002/2016GL071636>
- Zheng, F., & Yu, J. Y. (2017). Contrasting the skills and biases of deterministic predictions for the two types of El Niño. *Advances in Atmospheric Sciences*, 34(12), 1395–1403. <https://doi.org/10.1007/s00376-017-6324-y>
- Zhou, L., & Zhang, R. H. (2022). A self-attention-based neural network for three-dimensional multivariate modeling and its skillful ENSO predictions. *Science Advances*, 9(10). <https://doi.org/10.1126/sciadv.adf2827>